Spectral behavior of high-power Compton free-electron lasers. I. Broadening and asymptotic equilibrium

D. Iracane, P. Chaix, and J. L. Ferrer*
Commissariat à l'Energie Atomique, Centre d'etudes de Bruyères-le-Châtel, Service de Physique et Technique Nucléaire, Boîte Postale 12, 91680, Bruyères-le-Châtel, France
(Received 22 April 1993)

We investigate the nonlinear spectral behavior of high-current Compton free-electron lasers. For that purpose, a multifrequency model is developed in the continuous-beam limit. Both numerical simulations and perturbation expansions allow us to point out a mechanism leading to a broadening of the spectrum. Then, we analyze the saturation and the asymptotic behavior of the spectrum corresponding to a large number of round-trips in the oscillator configuration. The existence of a stable asymptotic regime presenting strong chaotic features is predicted. In this regime, efficiency is provided by a diffusionlike behavior of the electrons rather than a standard synchrotron motion. Consequently, we show that the efficiency and the spectral width can be evaluated simply and in closed form: they behave like the square roots of the electron density, of the wiggler length, and of the cavity quality factor.

PACS number(s): 41.60.Cr, 52.35.Mw, 52.35.Ra

I. INTRODUCTION

High-power Compton free-electron lasers (FEL's) are characterized by very involved nonlinear behaviors, leading to saturation and eventually to equilibrium. The underlying physics belongs to a wide class of problems involving couplings linear in the radiation field and periodic in the electron positions (intermodulation in traveling-wave tubes, Langmuir waves in plasmas [1], etc.). However, these phenomena are mainly understood in the linear low-field and low-gain regime (the Madey regime for FEL's, the quasilinear regime for Langmuir waves, etc.). In a previous Letter [2], we pointed out two results about the nonlinear regime. First, by computing in closed form the third-order term in a perturbation expansion, we showed how new frequencies appear in the FEL spectrum. Second, by using a full numerical simulation, we characterized the asymptotic equilibrium by a scaling law exhibiting a universal ratio between the extracted efficiency and the relative spectral width. The present paper goes further by presenting a more detailed analysis of the perturbation expansion and an interpretation of the asymptotic equilibrium leading to simple evaluations of the efficiency and spectral width.

The model we use (Sec. II) describes the spectral dynamics around a fundamental frequency with a restricted two-dimensional (2D) analysis. Since the nonlinear multifrequency physics is expected to provide very intricate behaviors, we will also briefly describe the computational scheme.

Through several perturbative expansions and simulations, we study the nonlinear coupling of an arbitrary number of longitudinal modes (Sec. III). This allows us to recover well-known processes, such as saturation or mode competition [3]. But we also observe other couplings, involving three or more longitudinal modes. Among these is a process which can be called difference-frequency generation (DFG) and is identified [2] as a source of new spectral lines. We characterize this mechanism within a third-order perturbation expansion computed in closed form. Then, with the help of numerical simulations, we verify that the DFG mechanism, starting from two or more strong laser modes, leads to a broad spectrum. Thus we sketch out a scenario where, starting from the well-known "fundamental-plus-sideband" situation, we finally get a broad spectrum. A more detailed analysis of the sideband instability and its relations to spectral broadening, including the effects of tapering, is presented in the following paper.

In the oscillator regime, full numerical simulations show that, beyond the spectral broadening due to the DFG, an asymptotic equilibrium takes place characterized by a spectral width much larger than the one predicted by the sideband instability (Sec. IV). This steady state is reached after a large number of round-trips, depending of course on the FEL parameters. We observe at saturation a proportionality between the spectral width and the extracted efficiency, which is consistent with high-current experiments [4,5]. Of course, such considerations are relevant as far as there is no frequency discrimination (filters). To get more insight into this asymptotic behavior, we analyze the stability of this equilibrium against various perturbations such as diffraction effects and tapering. The broad-spectrum-regime equilibrium appears to be very stable. Finally, we clarify this universal behavior by investigating the electron dynamics in a broad spectrum laser. By using a simple Fokker-Planck description, we predict the performances of high-power FEL's versus electronic charge, wiggler length, and cavity losses. The laws describing this regime are very different from the usual laws relevant for the standard monochromatic-laser regime [Eq. (41)]. These results are of practical importance since they show that the FEL efficiency can be made typically one order of magnitude larger in the broad-spectrum regime than in the monochromatic regime.

II. MODELING AND NUMERICAL SCHEME

The paraxial approximation makes it possible to model the electric field of a FEL by a complex field satisfying a time-dependent Schrödinger equation, where the electronic current acts as an inhomogeneous source term. We describe radial effects in a simplified way by coupling a 2D laser beam to a 1D cylindrical electron beam with a static radial profile [6]. Numerical simulations based on this mixed 1D-2D model conserve energy and take into account guiding effects with moderate computer CPU time, for example, by expanding the laser field on a finite radial basis [7]. Then, it is possible to address the spectral dynamics by expanding the 2D laser field over a discrete sequence of longitudinal modes.

We study FEL spectral dynamics in the continuous-beam limit which is relevant for electronic pulses much longer than the slippage distance [8]. This means that finite-pulse issues, such as natural Fourier spread or temporal overlap effects, are disregarded. The laser field A_L is expanded as the product of rapid phases and slowly varying envelopes $\mathcal{E}_n(r,z)$:

$$A_L=\frac{mc}{e}\mathrm{Re}\left[\sum_{n\,(\ll N)}\frac{\mathcal{E}_n(r,z)}{k_n}e^{ik_n(z-ct)}\right], \tag{1}$$

where m and $-e$ are the electron mass and charge, and r is the radial distance from the z axis. The wave number k_L is an arbitrary reference and $k_n=(1+n/N)k_L$ is assumed to be close to the central mode k_L ($n\ll N$). Each complex laser field $\mathcal{E}_n$ satisfies a paraxial equation resulting from the Maxwell equations:

$$i\partial_z\mathcal{E}_n=-\frac{\Delta_\perp}{2k_n}\mathcal{E}_n+\mu_0e^2ca_w\mathcal{H}_1T(r)\int_1^{+\infty}d\gamma\frac{1}{2\pi N}\int_0^{2\pi N}d\psi\,g(z,\psi,\gamma)\tfrac{1}{2}\exp[-i\psi_n]/\gamma\ , \tag{2}$$

where $\Delta_\perp=\partial_x^2+\partial_y^2$ is the transverse Laplacian operator, γ is the kinetic energy of electrons normalized to mc^2, a_W is the normalized wiggler magnetic-field amplitude and k_W its wave number, $\mathcal{H}_1$ is the usual coupling parameter [9], and $T(r)$ is the electron-beam profile which is assumed to be constant and normalized according to $\int 2\pi r\,dr\,T(r)=1$.

The longitudinal electronic phase space is characterized [10] by the resonant phase $\psi=(k_L+k_w)z-ck_Lt$ and the kinetic energy γ. The variable ψ depends on the central wave number k_L, but the dynamical equations are invariant under the choice of k_L when we consider the limit of the continuous Fourier expansion in Eq. (1). Indeed, the phase

$$\psi_n=\left[1+\frac{n}{N}\right]\psi-\frac{n}{N}k_wz=(k_w+k_n)z-ck_nt\ , \tag{3}$$

appearing in Eq. (2) is precisely the resonant phase for the wave number k_n. The longitudinal electronic distribution $g(z,\psi,\gamma)$ satisfies the associated Vlasov equations:

$$\left[\partial_z+v\partial_\psi+\Gamma\left[\partial_\gamma-\frac{1}{\gamma}\right]\right]g(z,\psi,\gamma)=0\ , \tag{4a}$$

$$v=k_w-\frac{k_L}{2\gamma^2}\left[1+\frac{a_W^2}{2}\right], \tag{4b}$$

$$\Gamma=a_w\mathcal{H}_1\mathrm{Im}\left[\sum_{m\,(\ll N)}\mathcal{R}_m\tfrac{1}{2}\exp[i\psi_m]/\gamma\right], \tag{4c}$$

and is normalized according to

$$\frac{1}{2\pi N}\int_0^{2\pi N}d\psi\int_1^{+\infty}d\gamma\,g(z,\psi,\gamma)mc=\rho_e\ . \tag{4d}$$

The density ρ_e is the electron number per unit of length and $\mathcal{R}_n$ is the radial self-consistent overlap between T and $\mathcal{E}_n$, i.e., the averaged laser field seen by the rigid radial section of the electron beam:

$$\mathcal{R}_n(z)=\int 2\pi r\,dr\,T(r)\mathcal{E}_n(r,z)\ . \tag{5}$$

The overlap $\mathcal{R}_n$ can be interpreted as a self-consistent filling factor, the evolution of which takes into account the competition between diffraction and optical guiding effects [7,11]. This partially 2D model is valid when the electron-beam radius is smaller than the laser-beam radius, which is a relevant assumption in our experiment [12]. This approximation is a projection, which implies energy conservation for the above set of equations. If E_e and E_L are, respectively, the electron and laser energies per unit of length, the sum E_e+E_L is constant:

$$E_e=mc\frac{1}{2\pi N}\int_0^{2\pi N}d\psi\int_1^{+\infty}d\gamma\,g(z,\psi,\gamma)mc^2\gamma\ ,$$

$$E_L=\frac{1}{2\mu_0}\left[\frac{mc}{e}\right]^2\int_0^{+\infty}2\pi r\,dr\sum_n\mathcal{E}_n\mathcal{E}_n^*\ .$$

The transverse Laplacian operator induces time-dependent phase shifts for each mode. For realistic parameters, these phase shifts vary slowly compared to the phase shifts due to longitudinal dynamics. Therefore, the major effect of the transverse dynamics is a geometrical effect described by the self-consistent filling factor. To make some complicated calculations more tractable, a 1D projection of the 2D dynamics is derived in the Appendix.

The term $(1/\gamma)g$ in Eq. (4a) is required for the conservation of the phase space volume and for the equivalence with the Newton equations:

$$d_z\psi=v\ ,\quad d_z\gamma=\Gamma\ . \tag{6}$$

This extra term can be exactly removed and the electron dynamics be made Hamiltonian by merely changing the phase-space coordinate γ into γ^2.

In fact, the models usually used for multifrequency simulations [13,14] work in position space [14], possibly with periodic boundary conditions [8,15,16]. In the limit

of continuous Fourier expansion, Eqs. (1)–(4) are physically equivalent to these models. The Fourier representation is well suited for the study of multifrequency mechanisms both for theoretical purposes [17] and numerical purposes since it allows a fine control of the initial spectrum and a precise tracking of each frequency. The laser field is expanded as a finite sequence of discrete Fourier modes so that the whole model Eqs. (1)–(4) is periodic with a period $N\lambda_L$ and the minimal distance between two laser wave numbers is $\delta k = k_L/N$. Typically, by using 50–100 modes with $N \geq 500$, we resolve spectral details with relative fractional widths $\geq 10^{-3}$ and within a bandwidth of few tens of percent (this must be compared with a sideband shift of a few percent).

To investigate new frequency generation mechanisms, it is necessary to perform simulations relevant for very low-amplitude fields. Two different issues have to be addressed.

First, a precise control of the total energy conservation is required to check that each electron trajectory is correct. To constrain the total energy conservation in simulation (simulation computer code SPECTRE) within the working precision of the computer, up to three or four digits, we have taken advantage of a basis expansion technique [7]. Then, by diagonalizing the Laplacian operator $\Delta_\perp$, it is possible to compute the unitary evolution operator $U(z)=\exp[i\Delta_\perp z/2k]$. We use this operator to define an interaction representation $\bar{\mathcal{E}} = U(z)\mathcal{E}$ for the electric field. Then we push particles and $\bar{\mathcal{E}}$ with a fourth-order Runge-Kutta scheme. The order of this algorithm is 4 since (i) we use an exact free evolution operator and (ii) the nonlinear part is treated by a fourth-order Runge-Kutta algorithm. This method is comparable to second-order algorithms used for solving time-dependent Schrödinger equations in nuclear physics [18].

Second, laser frequency generation is relevant or not depending on the statistical properties of the numerical sampling. Let us consider $\mathcal{N}_e$ electrons equally spaced in a $2\pi N$ phase space. Depending on the ratio $\mathcal{N}_e/N$, some electrons can get very close to a separatrix in the phase space. In that case, the status of this electron can change easily from bound to unbound. This generates localized perturbations of the order $1/N_e$, which means in the frequency space a white noise. A precise control of noise allows an important cross validation between numerical simulations and perturbative calculations and also gives the opportunity to extend the analytical analysis into a more complex and realistic investigation.

This second point is the key issue of multifrequency simulations. When the laser spectrum is simple enough (for example, when it is characterized by one or two dominant modes), it is possible to control precisely the noise at a level comparable to the computer precision. This can be achieved by optimizing the initial electron sampling along the ψ axis, i.e., the distribution of the N_e equidistant particles in a $2\pi N$ long box. This can be illustrated when there is a dominant mode, say k_L. The equations are basically 2π periodic. Moreover, if m_1 is the highest common integer factor of $\mathcal{N}_e$ and N, the sampling of the initial condition, and then the whole dynamics, is $2\pi m$ periodic where $m = N/m_1$. This implies that any noise mechanism will generate a modulation with wavelength smaller than $2\pi m$, which means wave number shifts larger than $\Delta k/k = 1/m = m_1/N$. In that case, we observe noise generation at the wave numbers $k_L(1+nm_1/N)$ with $n=1,2,\ldots$. So by increasing the symmetry of the initial sampling, we push the noise outside from the considered spectral bandwidth (m_1 larger than the number of simulated modes). We have successfully used this technique to test the DFG where two initial dominant modes are initially present (see Sec. III, Figs. 1 and 4). This technique can be generalized when three or more frequencies are dominant but the resulting $\mathcal{N}_e$ increases dramatically. Then, it is not possible to make use of this simple arithmetic rule to prevent noise generation in the most general case. Moreover, at saturation and for a broad laser spectrum, the potential seen by the electrons is very complicated: it is the sum of many periodic potentials with time-dependent relative phases. This induces a high sensitivity to initial conditions. Therefore, it is not relevant to focus on precise details of the spectral evolution and we will chiefly analyze mean values such as the efficiency or the spectral mean square width (see Sec. IV).

III. PERTURBATIVE ANALYSIS OF THE SPECTRAL BROADENING

Nonlinear couplings occur when the laser field, or the periodic modulation of the electronic distribution, becomes strong enough. In such a case, the evolution of laser modes differs from that given by the linear gain curve. The most common illustration of these nonlinear effects is the self-saturation of the fundamental mode. This situation also occurs with the sideband or trapping instability [10] due to the synchrotron rotation of electrons. A large part of the following paper is devoted to the analysis of this instability in a realistic spectral evolution.

Moreover, one can expect that any beating wave, resulting from a linear combination of laser frequencies, can itself be amplified if it corresponds to an excitable frequency of the system. For example, the electronic distribution, when modulated by several laser modes, generates source terms containing combinations of these modes. New modes can be either amplified from noise or created from a zero-energy level. This section is devoted to an analytical analysis of these processes. Since the following computations are quite intricate, we assume that diffraction can be switched off, and we consider Gaussian beams in the 1D limit (Appendix). Radial profiles are frozen: $T(r)=\exp(-r^2/r_e^2)/\pi r_e^2$ for the electronic beam and $S(r)=\exp(-r^2/2r_L^2)/(\pi r_L^2)^{1/2}$ for the laser beam. Equations (2) and (4c) become

$$\partial_z \gamma = \Gamma = a_w \mathcal{H}_1 \langle ST \rangle (\pi r_L^2)^{1/2} \mathrm{Im}\left[\sum \mathcal{E}_n \exp(i\psi_n)/2\gamma \right] , \tag{7}$$

$$i\partial_Z \mathcal{E}_n = \frac{\mu_0 e^2}{m} a_w \mathcal{H}_1 n_e \langle \exp(-i\psi_n)/2\gamma \rangle , \tag{8}$$

where $n_e = \rho_e/\pi r_e^2$ is the electron number per unit of

volume at $r=0$ and $\mathcal{E}_n(z)=\mathcal{E}_n(r=0,z)$ is the value of the 2D laser field (Sec. II) on the axis. The mean value $\langle\ \rangle$ in Eq. (8) is defined with the electronic distribution g normalized by Eq. (4d). This 1D limit is valid when the phase shift $L_w/2r_e^2k_L$ induced by the radial Laplacian operator is small compared to 1. In this section, we assume for simplicity a perfect radial overlap between the electronic density and the laser field, that is, we limit ourselves to $r_e^2=2r_L^2$. In this case, one has $\langle ST\rangle(\pi r_L^2)^{1/2}=\frac{1}{2}$.

The origin of the frequency generation by a direct coupling of laser modes can be clarified within perturbation theory. By giving in a closed form an explicit calculation up to the third order, we will exhibit mechanisms for mode coupling which are clearly responsible for the spectral broadening. To begin with, it is necessary to fix the formal frame of this perturbative expansion. Indeed, to make the analysis tractable, two small parameters are required: the electron density and the electric field $\mathcal{E}$. This comes from the fact that the source term for the Vlasov equation (the Maxwell equation) is given by the laser intensity (the electronic density). This well-known structure of the Vlasov-Maxwell equations allows us to sketch out the structure of the expansion. Then, we will focus on terms in the weak-current limit (first order in the electronic density) and in the low-field limit (up to the third order in the laser field). This means that we provide the explicit formula that generalizes the Madey gain theorem [19]. This will be relevant for weak electronic currents or for short undulators. Comparison with full simulations will give the validity range of this third-order approximation.

To label the different orders of this two-parameter expansion, we introduce a double index (i,j), where i is related to the electronic density and j to the laser strength. For any perturbation order (i,j), we can define the electronic density, the laser field, and the driving term of the Vlasov equation, respectively,

$$g^{(i,j)}\ ,\quad \mathcal{E}_n^{(i,j)}\ ,\quad \Gamma^{(i,j)}\ . \tag{9}$$

By definition, at the order $i=0$, there is no electron, which implies $g^{(0,j)}=0$ for any j. In the same way, the zero order in the laser field means that $\mathcal{E}_n^{(i,0)}=0$, so that $\Gamma^{(i,0)}=0$, for any i. Moreover, when there is no electron $i=0$ (no photon $j=0$), the laser field (the electronic density) does not evolve, which means that $\mathcal{E}_n^{(0,j)}$ ($g^{(i,0)}$) are constant and are given by the initial conditions. These constants are zero for i or j strictly greater than 1, because in the absence of interaction, the high-order terms are meaningless. This simple analysis provides the initial values for the following general recursion law deduced from the Vlasov equation Eq. (4):

$$\begin{aligned}(\partial_z+v\partial_\psi)g^{(i,j)}=&-\sum_{\substack{0<p<i\\0<q<j}}\Gamma^{(p,q)}\left[\partial_\gamma-\frac{1}{\gamma}\right]g^{(i-p,j-q)}\\&-\Gamma^{(0,1)}\left[\partial_\gamma-\frac{1}{\gamma}\right]g^{(i,j-1)}\\&-\Gamma^{(i-1,j)}\left[\partial_\gamma-\frac{1}{\gamma}\right]g^{(1,0)}\ .\end{aligned}\tag{10}$$

It should be noticed that neither $g^{(i,j)}$ nor $\mathcal{E}^{(i,j)}$ is present in the summation, so that Eq. (10) allows a direct calculation of $g^{(i,j)}$ by a simple integration. Knowing $g^{(i,j)}$, one can then deduce $\mathcal{E}^{(i,j)}$ by another integration over the wiggler length L_w:

$$\begin{aligned}i\partial_Z\mathcal{E}_n^{(i,j)}=&\frac{\mu_0e^2ca_w\mathcal{K}_1}{\pi r_e^2}\\&\times\int_1^{+\infty}d\gamma\frac{1}{2\pi N}\int_0^{2\pi N}d\psi\,g^{(i,j)}(z,\psi,\gamma)\frac{1}{2\gamma}\\&\times\exp(-i\psi_n)\ .\end{aligned}\tag{11}$$

The driving force is then deduced from Eq. (7):

$$\Gamma^{(i,j)}=a_w\mathcal{K}_1/2\,\mathrm{Im}\left[\sum\mathcal{E}_n^{(i,j)}\exp(i\psi_n)/2\gamma\right]\ . \tag{12}$$

The initial condition is a monoenergetic uniform infinite e beam:

$$g^{(1,0)}=\frac{1}{mc}\rho_e\delta(\gamma-\gamma_0) \tag{13}$$

and an initial laser energy split in several modes $\mathcal{E}_n^{(0,1)}$ with $n\in\{n_1,\ldots,n_r\}$. At the first order, we get the weak-field, low-gain, amplification rate:

$$i\partial_Z\mathcal{E}_n^{(1,1)}(z)=x_n(z)\mathcal{E}_n^{(0,1)}(0) \tag{14}$$

with

$$\begin{aligned}x_n=&-\mu_0\frac{e^2}{8m}a_w^2\mathcal{K}_1^2n_e\frac{1}{\gamma_0^3}e^{i(n/N)k_wz}\\&\times\left[\frac{1}{2i}\phi_n+k_w\left[1+\frac{n}{N}\right]\int_0^zdz_1\phi_n\right],\\\phi_n(z)=&\frac{e^{-i(n/N)k_wz}-1}{-i\dfrac{n}{N}k_w}\ .\end{aligned}$$

By direct integration, we get the usual Madey formula [20] for the weak-field and low-gain limit:

$$g=\Delta E_l/E_l=I\partial_\varphi\left[\frac{\sin^2\varphi}{\varphi^2}\right] \tag{15}$$

with

$$I=\mu_0(e^2/16m)a_w^2\mathcal{K}_1^2n_e(1/\gamma_0^3)k_wL_w^3,\quad \varphi=\nu_0L_w/2\ .$$

At second order, there is no resonant contribution close to the initial frequencies (the smallest resonant frequency will be close to the second harmonic of the initial modes, but this is outside the scope of this analysis). The first relevant contribution appears at third order in the laser field. At this order, the laser field evolution equation can be written with a force term, from which the electronic degrees of freedom are completely removed:

$$i\partial_Z \mathcal{E}_n^{(1,3)}(z)=\mu_0\frac{e^2}{2m}\mathcal{H}_1 a_w n_e \frac{1}{\gamma_0}\frac{1}{2\pi N}e^{i(n/N)k_w z}\int_0^{2\pi N}d\psi\, e^{-i(1+n/N)\psi}J_{(3)}\ ,$$

$$J_{(3)}=-\frac{1}{\gamma_0^6}\left[\tfrac{5}{2}V^3+k_w\left[15\partial_\psi\int_0^z dz_1 V^3+10\int_0^z dz_1 U\partial_\psi\int_0^{z_1}dz_2 V^2+6\int_0^z dz_1 U\int_0^{z_1}dz_2 U\partial_\psi\int_0^{z_2}dz_3 V\right]\right.$$
$$+k_w^2\left[20\partial_\psi^2\int_0^z dz_1\int_0^{z_1}dz_2 V^3+32\partial_\psi\int_0^z dz_1\int_0^{z_1}dz_2 U\partial_\psi\int_0^{z_2}dz_3 V^2\right.$$
$$+24\partial_\psi\int_0^z dz_1\int_0^{z_1}dz_2 U\int_0^{z_2}dz_3 U\partial_\psi\int_0^{z_3}dz_4 V$$
$$\left.+4\int_0^z dz_1 U\partial_\psi\int_0^{z_1}dz_2\partial_\psi\int_0^{z_2}dz_3 V^2+4\int_0^z dz_1 U\partial_\psi\int_0^{z_1}dz_2\int_0^{z_2}dz_3 U\partial_\psi\int_0^{z_3}dz_4 V\right]$$
$$+k_w^3\left[8\partial_\psi^3\int_0^z dz_1\int_0^{z_1}dz_2\int_0^{z_2}dz_3 V^3+16\partial_\psi^2\int_0^z dz_1\int_0^{z_1}dz_2\int_0^{z_2}dz_3 U\partial_\psi\int_0^{z_3}dz_4 V^2\right.$$
$$+16\partial_\psi^2\int_0^z dz_1\int_0^{z_1}dz_2\int_0^{z_2}dz_3 U\int_0^{z_3}dz_4 U\partial_\psi\int_0^{z_4}dz_5 V+8\partial_\psi\int_0^z dz_1\int_0^{z_1}dz_2 U\partial_\psi\int_0^{z_2}dz_3\partial_\psi\int_0^{z_3}dz_4 V^2$$
$$\left.\left.+8\partial_\psi\int_0^z dz_1\int_0^{z_1}dz_2 U\partial_\psi\int_0^{z_2}dz_3\int_0^{z_3}dz_4 U\partial_\psi\int_0^{z_4}dz_5 V\right]\right]\ , \tag{16}$$

where $U(z,\psi)=\gamma\Gamma^{(0,1)}$ is readily obtained from Eq. (12) and $V(z,\psi)=\int_0^z dz' U(z',\psi)$. This lengthy expansion of the driving forces between laser frequencies exhibits resonant contributions as a sum of products:

$$\mathcal{E}_p^{(0,1)}(z_1)\mathcal{E}_q^{(0,1)}(z_2)\mathcal{E}_m^{(0,1)*}(z_3)\ ,$$

taken at $z_1=z_2=z_3=0$. This can interpreted as the first-order perturbation expansion of a Φ^4 field theory involving a tensor kernel $\mathcal{V}_{n,m,p,q}(z,z_1,z_2,z_3)$ with the following properties: (i) the kernel is nonlocal in time ($z_1\neq z$); (ii) the kernel is zero for z_1,z_2,z_3 larger than z (causality); (iii) the kernel couples frequencies with $n+m=p+q$ (momentum conservation). The explicit form of the kernel may be obtained by a functional derivation of $J_{(3)}$ with respect to $\mathcal{E}_n^{(0,1)}$. Hence this third-order calculation provides an effective interaction between laser frequencies, obtained by the explicit elimination of the electronic degrees of freedom:

$$i\partial_z \mathcal{E}_n^{(1,3)}(z)=\sum_{\substack{p,q,m\in\{n_1,\ldots,n_r\}\\ n+m=p+q}}\mathcal{V}_{n,m,p,q}\mathcal{E}_p^{(1,3)}(z_1)\times\mathcal{E}_q^{(1,3)}(z_2)\mathcal{E}_m^{(1,3)*}(z_3) \tag{17}$$

with $\mathcal{E}_p^{(1,3)}(z=0)=\mathcal{E}_p^{(0,1)}$.

The above nonlinear Φ^4 Schrödinger equation governs the laser dynamics up to the first order in the current. This illustrates the intrinsic complexity of the coupled system Eqs. (7) and (8).

The above first-order term in the current expansion involves a convolution between the kernel $\mathcal{V}$ and laser fields $\mathcal{E}_n^{(0,1)}$ assumed to be constant along the wiggler. Higher-order terms in the current take into account the variation of the laser field and can be obtained by using, in the right-hand side term, the value of the field previously calculated by solving Eq. (16) at the first order of the current. The third-order formula Eq. (16) takes into account different physical mechanisms (all the cases are listed in Table I): self-saturation, cross saturation, and difference-frequency generation. In the following, we focus our attention on the term $\mathcal{E}_p^{(0,1)}\mathcal{E}_q^{(0,1)}\mathcal{E}_m^{(0,1)*}$ altering $\mathcal{E}_n^{(1,3)}$ following Eq. (16).

The case $n=m=p=q$ corresponds to self-saturation. The third-order term only describes the beginning of the gain collapse. However, the comparison with a full numerical simulation (Fig. 1) shows the good accuracy of the computation with Eq. (16) (the perturbation expansion is evaluated exactly by using a symbolic computer code written in MATHEMATICA). The variation of the gain can be described by the third-order theory over a large range of laser energies (i.e., two decades above the linear regime). Beyond the quantitative evaluation of Eq. (16), it is worthwhile to provide a qualitative analysis to investigate the beginning of the nonlinear regime depending on the value of the electric laser field. For fields larger than some threshold $\mathcal{E}_{\rm NL}$, high-order terms are required to describe the FEL evolution. Then, $\mathcal{E}_{\rm NL}$ gives the validity range of the Madey theorem. In order to get an estimate for this threshold between linear and nonlinear regimes, we simplify Eq. (16) by considering two opposite cases depending on the frequency shift $\delta k/k$ between the spontaneous emission frequency $k_{\rm sp}$ and the laser frequency k_L.

(i) In the first regime, the difference between the electron-beam energy γ_0 and the resonant electron energy γ_R is much smaller than the resonance width, which means that we consider electrons trapped in the ponderomotive potential wells. This condition can be rewritten $k_w L_w(\delta k/k)\ll 1$. Then the phases $\kappa z=(\delta k/k)k_w z$ can be neglected in Eq. (16), so that $\int dz\exp(i\kappa z)\simeq L_w$. Now, the ratio between any successive nonlinear orders

(and not only between the third and first orders) becomes close to unity for

$$\mathcal{E} \sim \mathcal{E}_{\rm sat} = 2\pi^2 \gamma_0^2 (a_w \mathcal{H}_1 k_w L_w^2)^{-1} . \quad (18)$$

The electric field $\mathcal{E}_{\rm sat}$ characterizes the saturation level since for $\mathcal{E} \sim \mathcal{E}_{\rm sat}$ all the perturbative terms are of the same order of magnitude. Moreover, we estimate that the linear regime is valid up to a threshold given by an electric field ten times smaller than $\mathcal{E}_{\rm sat}$, so that we define a second scale $\mathcal{E}_{\rm NL}$ as the limit of validity of the first perturbation order: nonlinear contributions are no more negligible for electric fields larger than $\mathcal{E}_{\rm NL}$.

$$\mathcal{E}_{\rm NL} = 2\gamma_0^2 (a_w \mathcal{H}_1 k_w L_w^2)^{-1} \simeq \mathcal{E}_{\rm sat}/10 . \quad (19)$$

To put the above expressions in a more intuitive form, we introduce the synchrotron frequency (assuming a monochromatic electric field $\mathcal{E}$):

$$\Omega^2(\mathcal{E}) = \mathcal{E} a_w \mathcal{H}_1 k_w / 2\gamma_0^2 . \quad (20)$$

Now, Eqs. (18) and (19) can be simply restated in terms of the synchrotron pulsation and the wiggler length L_w:

$$L_w \Omega(\mathcal{E}_{\rm NL}) \cong 1 , \quad L_w \Omega(\mathcal{E}_{\rm sat}) \cong \pi . \quad (21)$$

We get here an expected result since Eq. (21) means simply that the linear regime is valid when the electrons run over a small fraction of the synchrotron rotation within the wiggler length and that the equilibrium at saturation is reached when the electrons run over a half a period of the synchrotron rotation within the wiggler length.

(ii) On the contrary, in the second regime, one assumes that the difference between the electron-beam energy and the resonant energy is larger than the resonance width. Here, to get a qualitative estimation of Eq. (16), one may replace the integrated trigonometric functions by their modulus, so that $\int dz \exp(i\kappa z) \simeq 1/\kappa$. This gives a new saturation level, now depending on $\delta k/k$:

$$\mathcal{E}'_{\rm NL} = \gamma_0^2 k_w \left[\frac{\delta k}{k} \right]^2 \Big/ (a_w \mathcal{H}_1) .$$

By using Eq. (20), this can be written

$$\Omega(\mathcal{E}'_{\rm NL}) = k_w \frac{\delta k}{k} / \sqrt{2} .$$

So, by using a drive laser to control $\delta k/k$, one would get a saturation energy which scales as the fourth power of the frequency shift between the laser frequency k_L and the spontaneous emission frequency $k_{\rm sp}$. Of course, one has to take into account the low-field-gain function which also depends on $\delta k/k$. For example, in the low-gain regime [Eq. (15)], it is well known that the maximum of gain is obtained for $k_w(\delta k/k)L_w = 2.6$. Then, for a frequency at the maximum gain, Eq. (21) gives $\Omega(\mathcal{E}'_{\rm NL}) = 1.8/L_w$. By taking into account the first-order gain curve, this second regime gives a threshold comparable to $\mathcal{E}_{\rm NL}$ and $\mathcal{E}_{\rm sat}$, up to a factor 2.

The validity of the above qualitative analysis is exemplified by Fig. 1. The threshold defined by the linear regime breakdown (or by the apparition of orders higher than 3) is in good agreement with the predicted one $\mathcal{E}_{\rm NL}$

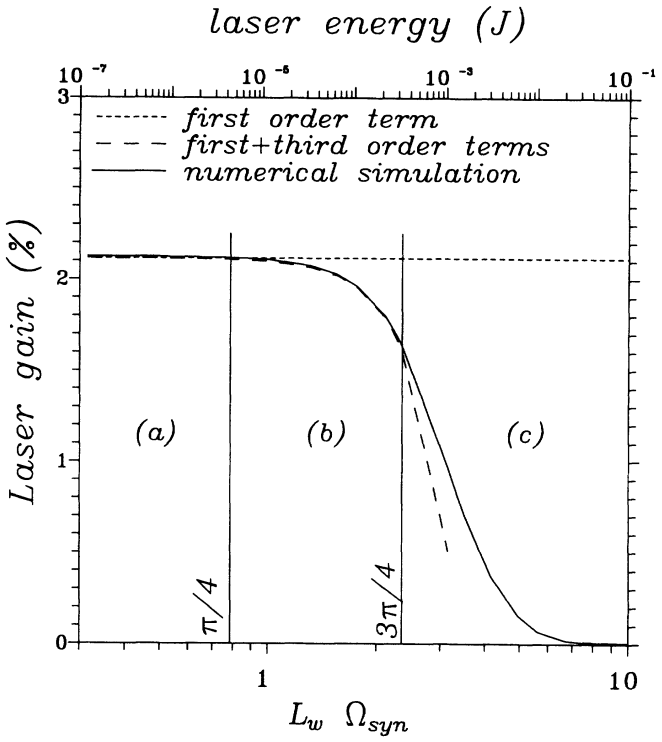

FIG. 1. Plot of the gain versus the laser energy, or equivalently the synchrotron frequency. The first-order perturbation term (Madey contribution) gives a constant value. Compared with a full numerical simulation, the third-order term fits correctly the beginning of the saturation. The areas (a), (b), and (c) give the validity range of the different contributions and are clearly connected to the fraction of synchrotron length run by the electrons through the wiggler.

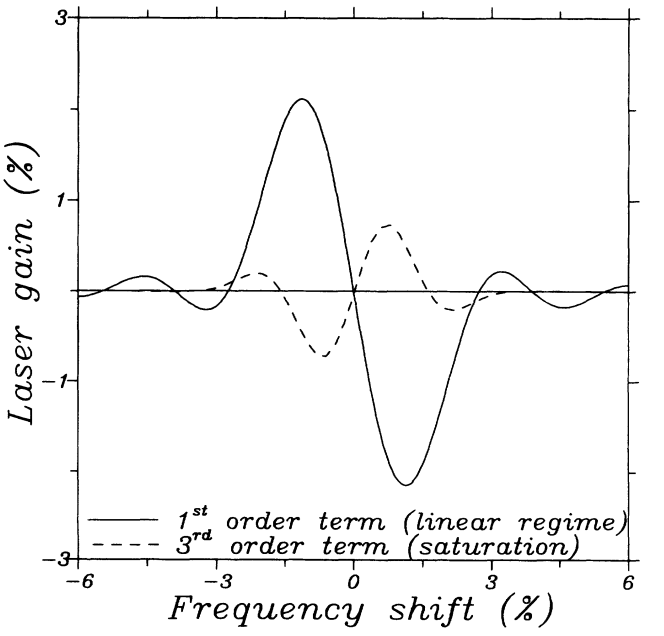

FIG. 2. Plot of the first-order and third-order contributions to the gain versus frequency. This provides the generalization of the usual Madey curve.

TABLE I. List of the mechanisms involved in the third-order term of the field perturbation expansion. The first-order term gives the Madey low-gain formula.

Case \ Number of pump modes (at third order)	1	2	3
Excited mode does not belong to the set of pump modes	$n=p=q=m$ (three terms) self-saturation	$p\neq q$, $m=p$ or $m=q$ (six terms) cross-saturation mode competition	$n=m=(p+q)/2$ (six terms) indirect mode competition
Excited mode belongs to the set of pump modes		$p=q$, $n=2p-m$ (three terms) DFG	n,p,q,m all distinct (six terms)

($\mathcal{E}_{sat}$). In Fig. 2 we show the first-order [Eq. (15)] and the third-order gain curves [Eq. (16)]. This simulation is performed with an electric field $\mathcal{E}$ corresponding to $L_w\Omega(\mathcal{E})\sim 3\pi/4$, which is the limit between regions (b) and (c) of Fig. 1. The effective gain for this value of the electric field is the sum of the two curves, which leads to a clear depletion of the maximum gain. This appears clearly on Fig. 3 where the summation of the first and third orders is plotted for different values of the electric field.

The case $n=p,q=m$ (or $n=q,p=m$) corresponds to the cross-saturation phenomenon and involves two modes that couple together. This can lead to a collapse of the weakest mode and may explain the sudden transition from a broad line to a sharp one at the end of the linear regime. The number of third-order terms contributing to cross saturation (six terms) is twice as large as those of self-saturation. This may lead to the quick conclusion that the cross-saturation phenomenon is twice as strong as the self-saturation [3]. However, the explicit evaluation of these terms shows that this is not generally true. This comes from the finite range of the effective interaction, which is responsible for a strong frequency dependence of its intensity. Hence an accurate third-order calculation must take into account all the phases due to the frequency differences. We face here a fundamental difference with [3] where an approximation of locality in time is assumed to simplify the evaluation of this third-order contribution. Such an approximation clearly breaks down when one deals with sideband modes, which is stated to be outside of the scope of [3]. Since we investigate mechanisms involved in broad spectrum regimes originating from sideband generation, it is essential to perform a full third-order calculation.

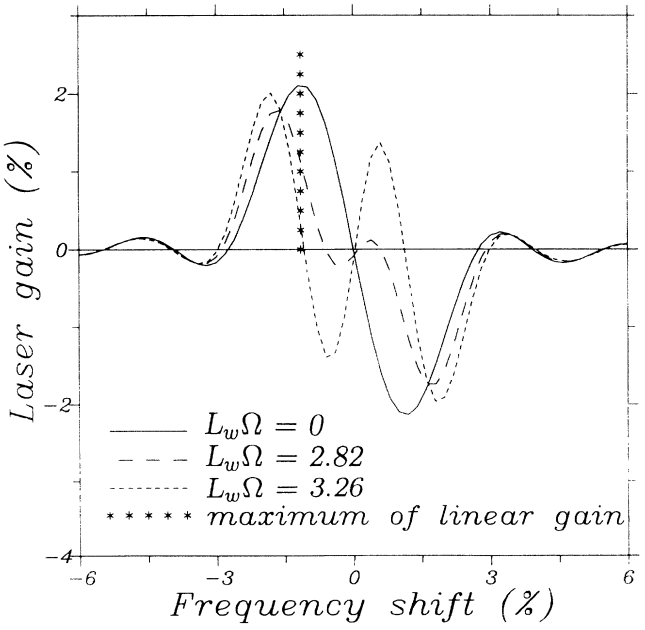

FIG. 3. Plot of the sum of the first- and third-order contributions to the gain versus frequency. The dotted vertical line corresponds to the frequency of maximum linear gain. The gain for this frequency goes to zero when the electric field increases up to $L_w\Omega_{syn}(\mathcal{E})\sim\pi$.

The case $p=q,n=2p-m$ corresponds to an interesting phenomenon, which can be called the difference frequency generation: two initial modes alter a third one. This may induce the growth of a new frequency from a zero-energy level. Since a two-line configuration is very common, because of the sideband instability, one may think that this phenomenon plays an important role in further spectral evolution. This can be made certain with the help of simulations. For example, one can consider a one-pass simulation where the fundamental mode and the sideband (centered, respectively, on k_f and k_s) are both present. We assume that the initial laser energy E_l is shared equally between k_f and k_s. The results of the numerical simulation are essentially given in Ref. [2]. The low noise level allows us to prove that all the modes $\mathcal{E}_n$, of wave number $k_n=k_f+n(k_f-k_s)$, where n is an integer, are amplified. This gives a well-suited interpretation of the spectrum evolution experimentally observed in [20], which can be compared with Fig. 1 of Ref. [2]. In both cases, the fundamental and sideband modes couple together to generate a DFG mode at the wave number $k_f-2(k_f-k_s)$. For high enough currents, the new modes k_n are amplified and can even dominate the initial modes k_f and k_s. In such cases, the new dominant mode can generate its own sideband k_s', which couples itself with k_f, k_s, and so on. A succession of sideband instabilities and DFG mechanisms leads ultimately to the

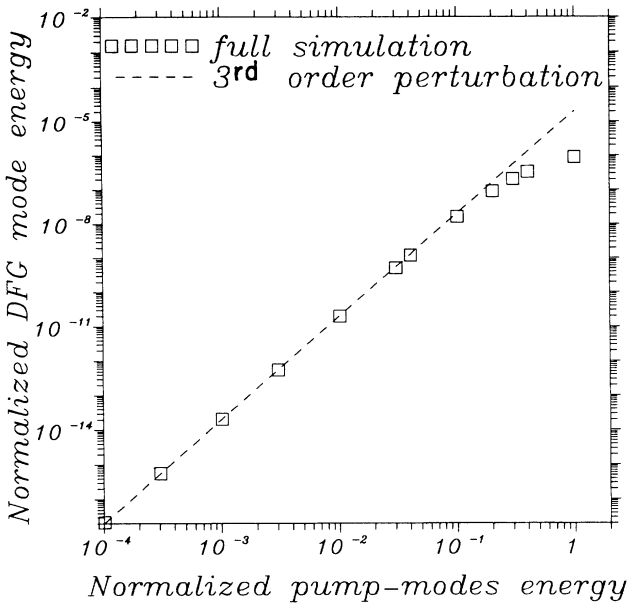

FIG. 4. Plot of the energy of the DFG modes versus the two-pump-mode energy. As expected, the slope of these curves is 3. The energies are normalized to the energy $E_{\rm sat}$ corresponding to $L_w\Omega_{\rm syn}(\mathcal{E}_{\rm sat})=\pi$. The third-order expansion is in perfect agreement with numerical simulations for the pump-mode energy smaller than $E_{\rm sat}$.

broadening and the densification of the spectrum. It appears that the perturbative expansion, compared with these numerical simulations, is very accurate for realistic physical parameters, showing that the DFG is not a numerical artifact. In Fig. 4 we point out that the third-order DFG, compared to a full simulation, is accurate for laser fields smaller than $\mathcal{E}_{\rm sat}$. The E_L expansion shows that the efficiency of the DFG mechanism depends on k_f and k_s. In Ref. [2], we have plotted the growth rate of the DFG, which appeared as a rapidly falling off function of $|k_f-k_s|$ with a width of a few percent full width at half maximum. As an essential feature, the present computation takes explicitly into account the frequency dependence with terms such as $\exp[i\psi(n/N)]$, which provide the frequency selection rules, and $\exp[i(n/N)k_wz]$, which control the intensity of the mechanism. When the interacting frequencies are very close, these phases can be taken equal to 1 over the wiggler length. But, dealing with the fundamental mode and its sideband leads to $k_wL_wn/N\simeq\pi$, which requires us to take precisely into account these phases. This is the case in our calculation which is relevant to test the coupling between the fundamental mode and its sideband.

In general, n, p, q, and m are all distinct. Such terms are important when the spectrum has many lines, and they might play a role in the structure of the fluctuations within the turbulent asymptotic regime. However, their qualitative analysis is less interesting in our context since they are not necessary to understand the beginning of the broadening.

The above analysis rests on a complicated expansion in the time-varying field variables. Purely time-dependent perturbation techniques are much more easily implemented: one expands the laser field as a Taylor series in the variable z, up to the third order. From a qualitative point of view, this expansion corroborates the above analysis: the first nontrivial term occurs at third order in the electric field and the harmonics $2k_f-k_s$ and $2k_s-k_f$ are amplified. The starting energy growth rate is proportional to $z^8E_l^3$. However, the comparison between this z expansion and the numerical simulation shows that the domain of validity of the z expansion is very small (a few millimeters). The scale of this drastic limitation is the wiggler period λ_w. Indeed, this scale appears in high perturbation orders through the variation of the longitudinal speed of the electrons with their energy $\partial_\gamma v$. It should be emphasized that the function vz is a slowly varying function compared to λ_w, but it is not the case for its derivative $\gamma\partial_\gamma vz\simeq k_wz$. Therefore, laser field expansions are the only suitable way to describe mode-coupling processes within perturbation theory. This example illustrates how the relevance of perturbation expansions strongly depends on the choice of the small parameter.

So, we have provided the effective interaction between laser frequencies after elimination of the electronic degrees of freedom, up to the third order.

IV. LONG-TIME EVOLUTION AND "UNIVERSAL" BRIGHTNESS

As explained in the preceding section, both perturbative expansions and low-power simulations show that the radiated spectrum widens following a two-step scenario: first, the well-known trapping instability causes the emergence of a sideband k_s close to the fundamental mode k_f; second, a sequence of harmonics of the difference k_f-k_s is generated. This process, which can be singled out within third-order perturbation theory, is the beginning of a more complex broadening due to higher-order couplings. Numerical simulations show that the new lines become as intense as the fundamental line and that they generate their own sideband instabilities. These new sideband lines couple with the already present ones, thus leading to more lines again by third-order frequency generation. This scenario explains not only the broadening of the spectrum, but also its densification. At that point, we have presented a quantitative estimation for the spectral evolution at low laser energy and low electron density and a qualitative analysis for the transient regime up to saturation. We will now study the saturation itself.

Computer simulations give us some insight in the long time (or large round-trip number) evolution of the spectrum. Let us first consider, for example, parameters related with an experiment [5] dealing with a 10-μm laser wavelength and an electronic current of the order of $J_e=200$ A. Simulations, assuming various values of J_e and of the cavity quality factor Q, in the continuous-beam limit, show various evolutions which all converge toward an asymptotic equilibrium [2]. A low current leads to a narrow spectrum; for higher currents, the spectrum is not only wider, but also more complicated since

the energy of each given mode is not constant: the energy seems to switch back and forth erratically from one frequency to another. Nevertheless, in all cases some average features of the spectrum, such as the total laser energy E_L or the relative spectral width $\Sigma=\sqrt{\langle k^2\rangle-\langle k\rangle^2}/k_L$, are quite stable in time. Simulations show that the relative width Σ at saturation increases with the electronic current J_e and the quality factor Q. Moreover, it appears that the spectral brightness $\mathcal{B}$, defined as the extracted efficiency per unit of relative frequency, remains largely independent of the control parameters characterizing the simulated experiment, as for example the current J_e, the quality factor Q (Fig. 5), or the wiggler length. While in the narrow spectrum regime, i.e., when the sideband is not fully developed, the spectral brightness is large and may vary by orders of magnitude from one case to the other, one always finds in the broad spectrum regime a spectral brightness of the order of, or slightly smaller than,

$$\mathcal{B}\equiv\frac{E_L}{QE_e\Sigma}\simeq 0.8\ . \tag{22}$$

The existence of such a "universal" spectral brightness means that high currents can make large efficiencies available, but only at the expense of a proportional spectral broadening.

It is important to note that our simulations have been carried out within an infinite-pulse hypothesis. Therefore, the comparison with experiments is valid only if these experiments have been performed with a large longitudinal overlap between the laser wave packet and the electron pulse. Indeed, in a finite-pulse FEL experiment, the spectral width may be controlled by the slippage effects and the optical cavity detuning [21,5], since the interaction time depends on the longitudinal overlap between the two beams. Moreover, the experimental qualitative behavior described in [5] is in perfect agreement with our simulations of the broad-spectrum regime. Indeed, the laser energy presents an erratic behavior, jumping from one frequency to another (see Fig. 3 of Ref. [2]). Another consequence of the universal brightness is the reduction of the efficiency when the laser is filtered either with some dispersive element [22,23] or via the optical cavity detuning [5,21]. Up to now, no dedicated measurement of the spectral brightness in the broad-spectrum regime has been available. But, using the experimental spectrum provided in [4], one gets a brightness equal to 0.8 ± 0.2, which is in good agreement with our statement (to obtain this result, we used the measured efficiency $\rho=1\pm0.2\%$ and we fitted the experimental spectrum as the sum of two Gaussians corresponding to the fundamental and sideband modes. The deduced relative rms width is 1.2%). The apparent universality of the spectral brightness numerical value for the broad spectrum regime typical of high power FEL's is not only a crucial result from an experimental point of view, since it implies that high efficiency is necessarily accompanied by spectrum broadening, but also from a theoretical point of view, since it suggests that there are important characteristics of the FEL dynamics which do not depend on most of the control parameters. The remainder of this section is therefore devoted first to a numerical analysis of the universality of the spectral brightness $\mathcal{B}$ in the broad spectrum regime, and second to its theoretical interpretation.

In order to test the stability of the asymptotic behavior, we performed various simulations and always found the same constant asymptotic spectral brightness $\mathcal{B}$ close to 0.8 in the broad spectrum regime.

In our simulation code SPECTRE, it is possible to switch on or off the diffraction terms due to the transverse Laplacian operator in Eq. (2) and the phase shifts due to the optical cavity (free propagation outside the wiggler and reflection on the mirrors). The simulations with or without diffraction lead to completely different evolutions of the laser phases. Nevertheless, we observe the same average spectral asymptotic regime, with the same constant brightness. From a theoretical point of view, this shows the nonsensitivity of the broad-spectrum regime on

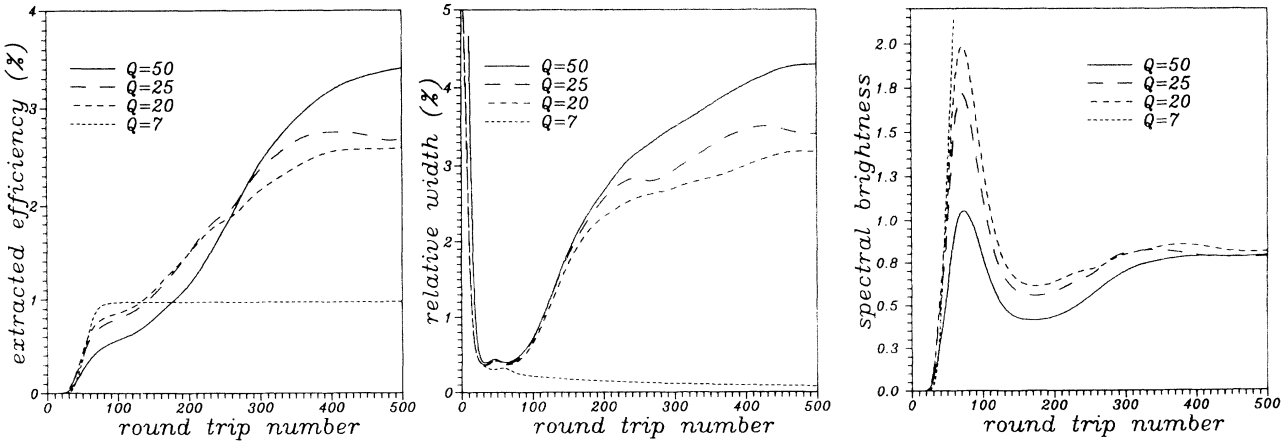

FIG. 5. Plots of the efficiency ρ, the relative width Σ, and the brightness $\mathcal{B}=\rho/\Sigma$ for various cavity quality factors Q. For $Q=7$, the losses are large and the spectrum remains monochromatic. The efficiency remains below 1% and the brightness becomes very large. For larger Q's, the spectrum broadens and the brightness reaches an asymptotic value $\mathcal{B}\simeq 0.8$ independent of Q.

strong phase perturbations, even though the detailed shape of the ponderomotive potential experienced by the electrons crucially depends on these phases.

Another way to try to disturb the spectral evolution is to inhibit the sideband instability by simulating a strong absorption around the sideband frequency. We found that this slows down the growth of new modes beyond the absorber, so that the asymptotic regime is delayed, but remains characterized by the same average features.

We also considered the effects of tapering. A tapered wiggler is designed with a decreasing mangetic field to enhance the efficiency [10]. Tapering is also expected to suppress sidebands [24]: an optimized tapering compensates the synchrotron rotation of the electrons in the ponderomotive potential well by a displacement of the resonance toward lower energies. Since the sideband instability originates from the synchrotron rotation, it is expected to be inhibited by an optimized tapering. However, reversing the point of view, the existence of broad spectra in high-power FEL's makes the tapering unlikely to be efficient since in such a regime, it is no longer possible to consider a simple phase-space structure with a well-defined resonance. For realistic high-power FEL's, tapering does not increase efficiency, due to strong spectral broadening. The only effect of tapering is then to delay the evolution because of a gain depletion. Thus, despite a large variation of the magnetic field along the wiggler, we get the same efficiency and the same brightness with or without tapering [25]. Such a result has been already forecasted from theory [26,8], but also experimentally observed [27]. An analysis of this important issue will be proposed in the companion paper.

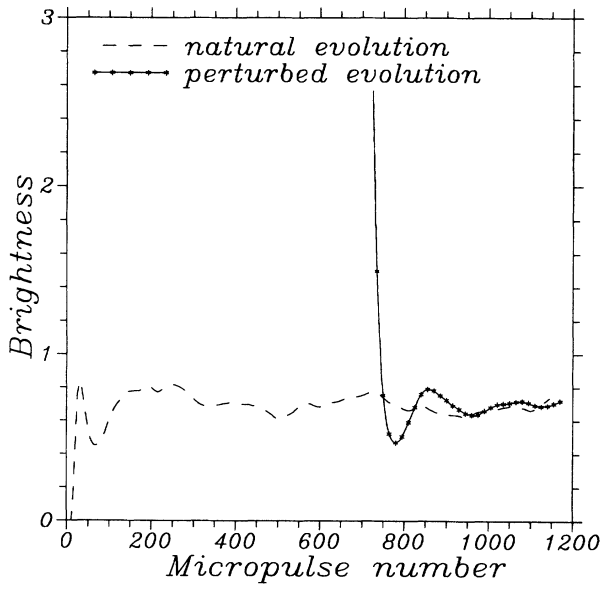

FIG. 6. Plot of the brightness $\mathcal{B}$ versus the round-trip number. The natural evolution for high-power FEL's leads to the universal value $\mathcal{B}\cong 0.8$. At the round-trip 600, we disturb the system by adding a large amount of laser energy on a given frequency, which increases the brightness. The asymptotic equilibrium is rapidly recovered.

Finally, we let the system evolve up to saturation and then induce a strong perturbation of the laser field. For example, we may spread the laser energy over a broader arbitrary spectrum or set all the laser phases to zero. In each case, we observe that the previous equilibrium is quickly recovered. In Fig. 6, for instance, we artificially increased the brightness by adding some additional laser energy on a given mode. We observe that it decreases back rapidly to its equilibrium value.

We may finally conclude that the system evolves toward a stable attractive asymptotic regime (saturation), presenting fluctuations around an average state characterized by an efficiency and a spectral width. Our aim is now to give the simplest possible description of this regime, in order to explain the universality of the spectral brightness, and to obtain evaluations of its average characteristics.

Since we consider the system at saturation, the gain is small (equal to the losses $1/Q$, a few percent). Therefore, for a given round-trip, the laser field amplitudes and phases may be considered as fixed. Because of the fluctuations, the phases ϕ_n may be considered as uniformly distributed and the amplitudes $|\mathcal{E}_n|$ as centered on a mean value $\langle|\mathcal{E}_n|\rangle$ varying smoothly with n. The wave numbers $k_n=(1+n/N)k_L$ range from a maximum $k_0\simeq k_L$ to a minimum $k_{\min}$ (the spectrum broadens toward smaller wave numbers), so that, with a smooth averaged spectrum, the relative spectral width is

$$\Sigma=\sqrt{\langle k^2\rangle-\langle k\rangle^2}/k_L=\frac{1}{2\sqrt{3}}\frac{k_L-k_{\min}}{k_L}\ . \tag{23}$$

Just like in Sec. III we will work with a 1D model where the radial profiles S and T of the electron and laser beams are frozen. However, we do not assume here that $r_e^2=2r_L^2$, so that we have to take into account the filling factor $\langle ST\rangle=\int 2\pi r\,dr\,T(r)S(r)$. Therefore, the dynamics of the electrons along the wiggler, for a given set of laser phases and amplitudes, is described by

$$\partial_z\psi=k_w(1-\gamma_R^2/\gamma^2)\ ,$$
$$2\gamma\partial_z\gamma=a_w\mathcal{H}_1\langle ST\rangle(\pi r_L^2)^{1/2}\times\sum_n|\mathcal{E}_n|\sin\left[\left[1+\frac{n}{N}\right]\psi-\frac{n}{N}k_wz-\phi_n\right]\ , \tag{24}$$

where $\mathcal{E}_n=|\mathcal{E}_n|\exp(-i\phi_n)$ and $\gamma_R^2\equiv k_L(1+\frac{1}{2}a_w^2)/2k_w$ is the square of the reduced energy resonant with the fundamental laser mode. Since we consider a broad-spectrum regime where the efficiency is much larger than in the monochromatic case, we can legitimately neglect the difference $\gamma_0-\gamma_R$ between the initial electron energy and the resonant energy for the fundamental mode: $\gamma_0^2\simeq\gamma_R^2$. Each term of the sum in Eq. (24) corresponds to a wave number $k_n=(1+n/N)k_L$ and generates a pendulumlike resonance in phase space, with a squared reduced energy γ_n^2 such that the phase $(1+n/N)\psi-(n/N)k_wz-\phi_n$ is constant. This writes, as a mere generalization of the well-known FEL resonance condition:

$$\gamma_n^2=\gamma_0^2\left[1+\frac{n}{N}\right]=\frac{k_n}{2k_w}(1+a_w^2/2)\ . \tag{25}$$

The structure of the motion of the electrons in this column of resonances depends on the field strength [28]. If the laser field were very small, each resonance would keep its identity, and electrons within the bucket associated to the nth mode will remain trapped around the corresponding energy γ_n. However, the separatrices of the buckets are blurred into stochastic layers. The thickness of these stochastic layers increases as the considered value of the strength is increased, up to a point where the resonances overlap and merge into a stochastic column coming down from γ_0 to $\gamma_{\min}$, with $\gamma_{\min}^2=k_{\min}(1+a_w^2/2)/2k_w$. In this regime of global stochasticity, the electrons are no longer confined in a given bucket. Their chaotic motion leads to an equipartition all over the available phase space. Let us now consider the electrons entering the wiggler when the large spectrum regime has been reached, due to sideband instabilities and nonlinear frequency generation. Their total initial energy per unit of beam length is

$$E_e=\rho_e\gamma_0 mc^2\ . \tag{26}$$

They experience a chaotic motion which eventually leads to an equipartition between the energies γ_0 and $\gamma_{\min}$, that is, to a total energy per unit of length $\frac{1}{2}\rho_e mc^2(\gamma_{\max}+\gamma_{\min})$. The energy variation for the electrons during their trip along the wiggler is therefore

$$\Delta E_e=\tfrac{1}{2}\rho_e mc^2(\gamma_{\min}-\gamma_0)\ . \tag{27}$$

Taking into account the relation Eq. (25) between the electron energies and the laser wave numbers, and the relation Eq. (23) between Σ and $k_L-k_{\min}$ one obtains

$$\Delta E_e\simeq-\frac{\sqrt{3}}{2}E_e\Sigma\ . \tag{28}$$

Since the total energy of the system electrons plus laser is conserved along the wiggler, the laser has increased its energy by an amount $\Delta E_L=-\Delta E_e=(\sqrt{3}/2)E_e\Sigma$; furthermore, since we are in the asymptotic equilibrium, this is just the energy extracted from the cavity $\Delta E_L=E_L/Q$, where Q is the optical cavity quality factor. Concatenating these simple equalities would lead to the spectral brightness $\mathcal{B}=E_L/(QE_e\Sigma)=\sqrt{3}/2\simeq 0.86$. Note that, following this interpretation, the transfer of electronic kinetic energy to the laser along the wiggler is no longer due to a coherent synchrotron motion of the electrons in a ponderomotive potential well, but rather to a chaotic diffusion toward lower energies. This is why in this regime the efficiency is no more related to the detuning $\gamma_0-\gamma_R$ (which we neglect here), but to the spectral width. More precisely, since the interaction time between the electrons and the laser is finite (it is given by the wiggler length), the equipartition between the energies γ_0 and $\gamma_{\min}$ is not complete at the wiggler exit, so that Eq. (27) slightly overestimates the electronic energy loss and only provides an upper bound for the brightness:

$$\mathcal{B}=\frac{E_L}{QE_e\Sigma}\le\frac{\sqrt{3}}{2}\simeq 0.86\ , \tag{29}$$

which is in agreement with the values issued from extensive numerical simulations. Actually, a complete prediction for $\mathcal{B}$ will need to take into account the self-consistent coupling of the laser to the electrons in the nonlinear regime, which is outside the scope of the present paper. However, we can use the fact that a laser mode k_n will be able to grow only if electrons are able to reach the corresponding resonant energy γ_n within the wiggler length. The electrons in the wiggler lose their energy by diffusion along the γ axis in the phase space, under the action of the broad-spectrum potential Eq. (24). The width of their energy distribution then evolves like $z^{1/2}$. Therefore, the electrons cannot couple to electromagnetic modes resonant with $\gamma\le\gamma_0-\beta L_w^{1/2}$, where β is some constant, that is, from Eq. (25) of wave number smaller than

$$k_{\min}=k_L\left[1-2\beta\frac{L_W^{1/2}}{\gamma_0}\right]\ . \tag{30}$$

Therefore the spectral width is controlled by the diffusion coefficient along the energy axis and by the wiggler length.

We can make this description more precise by deriving an expression for the diffusion coefficient around each energy γ. Let us then pick up a given mode n and consider the resonant electrons with $\gamma\simeq\gamma_n$. It is then preferable to use the variable ψ_n [Eq. (3)] for the electron phase, so that Eq. (24) becomes (with $n\ll N$)

$$\partial_z\gamma=a_w\mathcal{K}_1\langle ST\rangle(\pi r_L^2)^{1/2}\frac{1}{2\gamma_n}\times\sum_m|\mathcal{E}_{n+m}|\sin\left[\left[1+\frac{m}{N}\right]\psi_n-\frac{m}{N}k_w z-\phi_{n+m}\right]\ . \tag{31}$$

We may first consider that the diffusion coefficient around γ_n depends only on the laser modes resonant with energies close to γ_n, that is, with $m\ll N$. We can then replace Eq. (31) by

$$\partial_z\gamma=a_w\mathcal{K}_1\langle ST\rangle(\pi r_L^2)^{1/2}\frac{1}{2\gamma_n}\times\sum_m|\mathcal{E}_{n+m}|\sin\left[\psi_n-\frac{m}{N}k_w z-\phi_{n+m}\right]\ .$$

We may now use the so-called quasilinear, or random-phase approximation which states that the dynamics rapidly decorrelates the phase ψ_n, so that it can be replaced by a uniform random variable Ψ. Then the energy γ obeys a stochastic differential equation:

$$\partial_z\gamma=a_w\mathcal{K}_1\langle ST\rangle(\pi r_L^2)^{1/2}\frac{1}{2\gamma_n}\times\sum_m|\mathcal{E}_{n+m}|\sin\left[\Psi-\frac{m}{N}k_w z\right]\ . \tag{32}$$

The evolution of the distribution function $g(z,\gamma)$ around γ_n can then be described by a Fokker-Planck equation [29]:

$$\partial_z g = \tfrac{1}{2}\partial_\gamma D \partial_\gamma g$$

$$\text{with } D(\gamma)=\frac{\langle \Delta\gamma^2\rangle}{\Delta z}=\frac{1}{\Delta z}\left\langle \left[\int_0^{\Delta z} dz\, \partial_z\gamma\right]^2\right\rangle , \quad (33)$$

where the expectation value $\langle\ \rangle$ must be taken over the electronic phase Ψ and over the field amplitudes $|\mathcal{E}|$. Up to the first order in the spectral width ($n \ll N$) one obtains a diffusion coefficient proportional to the spectral energy density of the laser:

$$D(\gamma_n)=\frac{\pi}{4}\frac{N}{k_w}(a_w\mathcal{H}_1\langle ST\rangle)^2(\pi r_L^2)\gamma_0^{-2}\langle|\mathcal{E}_n|^2\rangle . \quad (34)$$

The asymptotic electronic energy profile $g(z,\gamma)$ does not depend on the shape of the spectrum: at large z the distribution will become uniform between γ_0 and $\gamma_{\min}$, resonant with k_L and $k_{\min}$. Furthermore, as long as the spectrum $\langle|\mathcal{E}_n|^2\rangle$ averaged on its fluctuations is smooth as a function of n, the time needed to reach the uniform final distribution depends very little on the details of the function $D(\gamma)$. This time is controlled by the first nonzero eigenvalue λ_1 of the Sturm-Liouville problem corresponding to the diffusion equation Eq. (33). This eigenvalue can be estimated [30] by $\lambda_1 \simeq -\pi^2[\int d\gamma\, D(\gamma)^{-1/2}]^2$, which is the same as if the diffusion coefficient were uniform with an effective value D defined by

$$D^{-1/2}\equiv\langle D(\gamma)^{-1/2}\rangle , \quad (35)$$

where $\langle\ \rangle$ is the mean value of $D(\gamma)$ between γ_0 and $\gamma_{\min}$. This eigenmode dominates the evolution toward equilibrium, since the next eigenvalue λ_2 can be evaluated in the same way to be four times larger than λ_1. Up to second order in the relative variations of the diffusion coefficient, Eq. (35) can be replaced by $D\equiv\langle D(\gamma)\rangle$ so that, within our approximations, everything happens as if the spectrum were uniform. This gives, with Eq. (34),

$$D=\frac{\pi}{4}\frac{1}{k_w}(a_w\mathcal{H}_1\langle ST\rangle)^2(\pi r_L^2)\gamma_0^{-2}\frac{1}{2\sqrt{3}\Sigma}\sum_n\langle|\mathcal{E}_n|^2\rangle .$$

Introducing the laser energy E_L [Eq. (A9) with a Gaussian profile] and the brightness $\mathcal{B}=E_L/(Q\gamma_0 mc^2\rho_e\Sigma)$, we finally obtain

$$D=\frac{\pi}{4\sqrt{3}}\frac{\mu_0 e^2}{m}\frac{(a_w\mathcal{H}_1\langle ST\rangle)^2}{\gamma_0 k_w}\mathcal{B}Q\rho_e . \quad (36)$$

Now, since the spectrum lies between k_L and $k_{\min}$, the electrons diffuse toward the lower energies in a stochastic column which is bounded by γ_0 and $\gamma_{\min}$. The frontiers of this region behave like reflecting walls so that, between γ_0 and $\gamma_{\min}$, the solution of Eq. (33) is the same as if the diffusion coefficient were uniform from $\gamma=-\infty$ to $+\infty$, but with an effective initial condition taking into account all the images γ_ν of the true initial condition γ_0 by reflection on these walls. This gives for $\gamma_{\min}\le\gamma\le\gamma_0$:

$$mcg(z,\gamma)=\rho_e\left[\frac{2}{\pi Dz}\right]^{1/2}\sum_{\nu\in Z}\exp\left[\frac{-(\gamma-\gamma_\nu)^2}{2Dz}\right] , \quad (37)$$

where $\gamma_\nu=\gamma_0+2\nu(\gamma_0-\gamma_{\min})=\gamma_0(1+2\nu\sqrt{3}\Sigma)$, so that

$$\langle\gamma(z)\rangle=\gamma_0-\frac{\sqrt{3}}{2}\Sigma\gamma_0\mathcal{G}\left[\frac{\sqrt{3}\Sigma\gamma_0}{(2Dz)^{1/2}}\right] , \quad (38)$$

with

$$\mathcal{G}(u)=\sum_{\nu\in Z}\left[\frac{2}{\sqrt{\pi}u}\{\exp-(2\nu u)^2-\exp-[(2\nu-1)u]^2\}\right.$$
$$\left.+4\nu\{\mathrm{erf}(2\nu u)-\mathrm{erf}[(2\nu-1)u]\}\right] .$$

The extracted efficiency is therefore related to the spectral width by

$$\rho=1-\frac{\langle\gamma(z=L_w)\rangle}{\gamma_0}=\frac{\sqrt{3}}{2}\Sigma\mathcal{G}\left[\frac{\sqrt{3}\Sigma\gamma_0}{(2DL_w)^{1/2}}\right] . \quad (39)$$

Introducing again the spectral brightness $\mathcal{B}=\rho/\Sigma$, we find that

$$\mathcal{B}=\frac{\sqrt{3}}{2}\mathcal{G}\left[\frac{\sqrt{3}\Sigma\gamma_0}{(2DL_w)^{1/2}}\right] . \quad (40)$$

The function $\mathcal{G}(u)$ is equal to 1 in the neighborhood of $u=0$, decreases, and behaves like $2/(\sqrt{\pi}u)$ when u goes to infinity. Therefore the value $\mathcal{B}=\sqrt{3}/2$ that we found in the preliminary treatment [Eq. (29)] is actually, as already stated, an upper limit of the spectral brightness in the broad spectrum regime.

One may obtain a first rough estimate of the efficiency by neglecting the fact that the stochastic column is bounded below at $\gamma_{\min}$. This can be done in a straightforward way from the diffusion equation Eq. (33), or more simply by taking $\Sigma=\infty$ in Eq. (39), so that the extracted efficiency is

$$\rho=\frac{1}{\gamma_0}\left[\frac{2}{\pi}DL_w\right]^{1/2} .$$

Taking into account Eq. (36), and, as another approximation, taking the brightness equal to its limit value $\mathcal{B}=\sqrt{3}/2$, the extracted efficiency and the corresponding relative spectral width are simply given by

$$\rho=\alpha(Q\rho_e L_w)^{1/2} , \quad (41a)$$

$$\Sigma=\frac{2\alpha}{\sqrt{3}}(Q\rho_e L_w)^{1/2} , \quad (41b)$$

with

$$\alpha^2=\alpha_0^2\equiv\frac{\mu_0 e^2}{4m}(a_w\mathcal{H}_1\langle ST\rangle)^2\gamma_0^{-3}k_w^{-1} . \quad (41c)$$

As expected, the extracted efficiency and the relative spectral width are both proportional to the square root of the wiggler length. But they are also proportional to the square root of the cavity quality factor and of the electron density. Note that the more we close the cavity, in-

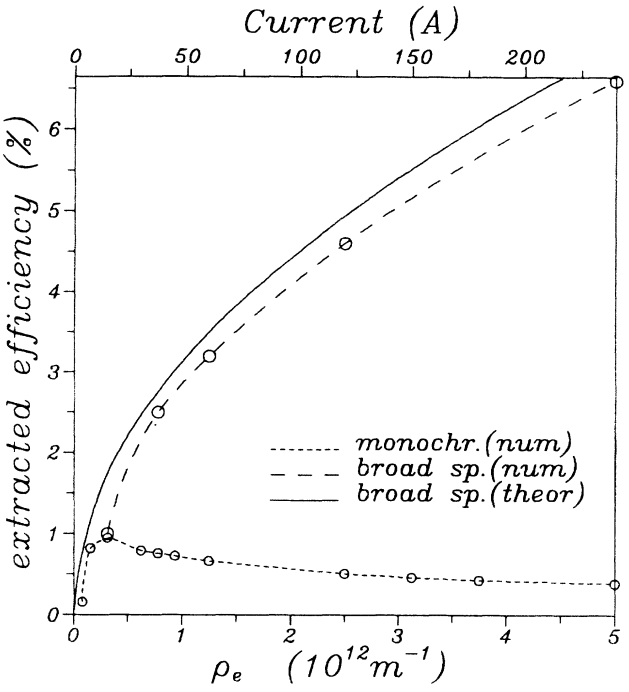

FIG. 7. Plot of the laser efficiency versus the electronic current. In the monochromatic case (dotted line), the efficiency is less than 1%, whatever the current. On the contrary, in the broad spectrum regime, the efficiency grows like the square root of the charge, so that it should reach 5% for existing devices. The numerical values for this set of simulations are [12] $a_w=1.075$, $\mathcal{K}_1=0.9$, $\lambda_w=2\pi/k_w=3.2$ cm, $\gamma_0=33$, $r_L=2$ mm, $r_e=1.5$ mm, $Q=25$, and $L_w=1$ m. Full simulations are in perfect agreement with the scaling law, Eq. (41a), providing, for the α coefficient $\alpha_{\text{num}}=5.72\times10^{-9}$ (broken line). The theoretical value obtained from Eq. (41d) gives a good estimate: $\alpha_{\text{th}}=6.12\times10^{-9}$ (solid line).

creasing Q, the more we extract energy [14] (see Fig. 5). Now taking into account the finite spectral width and the precise value of the spectral brightness, we simply find from Eqs. (39) and (40) that the theoretical value of the α coefficient is renormalized by a factor smaller than 1:

$$\alpha_{\text{th}}=\alpha_0\frac{\sqrt{\pi}}{2}\left[\frac{2\mathcal{B}}{\sqrt{3}}\right]^{3/2}\mathcal{G}^{-1}\left[\frac{2\mathcal{B}}{\sqrt{3}}\right]. \tag{41d}$$

The laws Eq. (41) have been tested by numerical simulations (Fig. 7). The simple formula Eq. (41c) gives the correct behavior and order of magnitude for the efficiency, while Eq. (41d), which needs the knowledge of the brightness, is in very good agreement with the full numerical simulations.

V. CONCLUSION

For high currents in the continuous-beam limit, we exhibited laser-mode couplings that lead to a spectrum larger than the classical sideband instability would let us think. These couplings, among them the difference-frequency generation, drive the nonlinear evolution of the laser from the sideband emergence to a broad-spectrum quasiequilibrium. We have provided a full perturbative analysis up to the third order in the field that generalizes the Madey theorem. Beyond the intricate formula obtained from this expansion, we give quantitative estimations for several of these third-order terms, but also a more qualitative evaluation that establishes the validity range of the linear and third-order terms.

Numerical simulation shows that the frequency generation mechanisms, exhibited within perturbation theory, are responsible for a strong broadening of the laser spectrum. The asymptotic regime is quite "turbulent," but can be characterized by some constant mean values, as the extracted efficiency ρ and the relative spectral width Σ. These asymptotic mean values depend on the FEL parameters, but simulations exhibit a "universal" constant: the spectral brightness $\mathcal{B}=\rho/\Sigma$, which is always found to be close to $\mathcal{B}\simeq0.8$. Miscellaneous numerical experiments were used to establish the stability of this behavior, which suggests some structural properties of the high-power FEL dynamics.

We made this idea more precise by providing a simple model exhibiting and taking into account the chaotic diffusion of particles in a broad spectrum potential. This model is able to explain most of the average properties obtained from heavy numerical simulations. The important point in our interpretation is that the amplitudes of the laser modes are large enough for the resonances to overlap, so that the electrons come down in phase space and lose enough energy to provide a large efficiency. It leads to scaling laws very different from the standard ones valid in the monochromatic regime. Now, the picture of FEL efficiency by chaotic diffusion should be made more complete, by taking into account the self-consistent coupling between the electrons and the laser. This is necessary if one wants to understand the transient regime, which has been, up to now, accessible only where perturbation theory is relevant, as described in Sec. III, and to derive a complete theoretical prediction for the spectral brightness. This would also enable us to reach a description of the dynamics of the laser phases and of the fluctuations in the asymptotic regime.

Beyond the fact that high-power FEL's appear to be interesting devices for experimenting fundamental nonlinear dynamics, we showed with both theoretical analysis and numerical simulations that a broad spectrum provides an efficient way to reach higher efficiencies. Indeed, Fig. 7 illustrates that the efficiency in the monochromatic case is limited whatever the electronic current. On the contrary, the efficiency in the broad-spectrum regime grows like the square root of the electronic charge.

APPENDIX: MODELING IN THE 1D LIMIT

As expected, the multifrequency behavior of high-power FEL's is a very intricate problem. Then, for particular investigations, it is helpful to switch off the two-dimensional dynamics. It is not possible to perform such a crude approximation in a canonical way. This means that the resultant set of equations depends on assumptions on the profile shape.

First, we need to use some radial form factor. Given

any function $F(x)$ defined on the positive real numbers with $F(0)=1$, we define the following integrals (supposed to converge):

$$I_1=2\pi\int_{x>0} x\,dx\,F(x)\ ,\quad I_3=2\pi\int_{x>0} x\,dx\,x^2F(x)\ ,$$
$$I_2=2\pi\int_{x>0} x\,dx\,F^2(x)\ ,\quad I_4=2\pi\int_{x>0} x\,dx\,x^2F^2(x)\ . \tag{A1}$$

Two typical functions are commonly used: the Gaussian

$$F(x)=\exp(-x^2)\ ,$$
$$I_1=\pi\ ,\quad I_2=\pi/2\ ,\quad I_3=\pi\ ,\quad I_4=\pi/4\ ;$$

and the step

$$F(x)=1_{[0,1]}\ ,$$
$$I_1=\pi\ ,\quad I_2=\pi\ ,\quad I_3=\pi/2\ ,\quad I_4=\pi/2\ .$$

Then, the electron-beam radial profile is given by

$$T(r)=\frac{I_3}{I_1^2r_e^2}F(\sqrt{I_3/I_1}\,r/r_e)\ , \tag{A2}$$

where r_e is the root-mean-square radius

$$\int 2\pi r\,dr\,T(r)=1\ ,\quad \int 2\pi r\,dr\,T(r)r^2=r_e^2\ . \tag{A3}$$

Similarly, the laser beam profile is

$$S(r)=\frac{\sqrt{I_4}}{I_2r_L}F(\sqrt{I_4/I_2}\,r/r_L)\ , \tag{A4}$$

where r_L is the root-mean-square radius

$$\int 2\pi r\,dr\,S^2(r)=1\ ,\quad \int 2\pi r\,dr\,S^2(r)r^2=r_L^2\ . \tag{A5}$$

We can now define a 1D electric field $\mathcal{E}(z)$ by the on-axis value of $\mathcal{E}(r,z)$:

$$\mathcal{E}(r,z)=\mathcal{E}(z)S(r)/S(0)\ . \tag{A6}$$

The one-dimensional limit is obtained when the radial scales go to infinity. Then, the Laplacian operator is switched off and, for finite radial distances, one can use $F\simeq 1$.

In a perfect 1D limit, the electric-field profile $S(r)$ is proportional to the electronic profile $T(r)$ [Eq. (2)]. Nevertheless, due to the different definitions of the mean values for the electron beam [Eq. (A3)] and the laser beam [Eq. (A5)], this implies different values for the rms radii. Typically, $r_e^2=2r_L^2$ for Gaussian profiles.

More generally, it is common to assume nondiffractive beams with different profiles leading to a nontrivial overlap $\langle ST\rangle$:

$$\langle ST\rangle\equiv\int 2\pi r\,dr\,S(r)T(r)\ . \tag{A7}$$

Since different scales may appear in S and T, it is not possible to give $\langle ST\rangle$ by using I_1 to I_4. For a Gaussian profile, we obtain

$$\langle ST\rangle=\frac{2}{\sqrt{\pi}}\frac{r_L}{r_e^2+2r_L^2}\ . \tag{A8}$$

With the above formula, the 1D model can be readily obtained from Eqs. (1)–(5). The averaged laser field [Eq. (5)] is simply $\mathcal{R}_n(z)=\mathcal{E}_n(z)\langle ST\rangle/S(0)$. The ratio $\langle ST\rangle/S(0)$ of the averaged to the on-axis laser field is a nondimensional filling factor equal to $2r_L^2/(r_e^2+2r_L^2)$ for Gaussian profiles. The laser energy per unit of length is now given by

$$E_L=\frac{1}{2\mu_0}\frac{m^2c^2}{e^2}\pi r_L^2\frac{I_2^2}{\pi I_4}\sum_n \mathcal{E}_n\mathcal{E}_n^*\ . \tag{A9}$$

One has to define the on-axis electronic density n_e as the electron number per unit of volume $n_e=\rho_eT(0)=\rho_eI_3/(r_e^2I_1^2)$. Then

$$id_z\mathcal{E}_n(z)=\frac{\mu_0e^2}{m}a_w\mathcal{H}_1n_e\langle\exp(-i\psi_n)/2\gamma\rangle\ , \tag{A10}$$

$$\partial_z\gamma=\Gamma=a_w\mathcal{H}_1\langle ST\rangle/S(0)\mathrm{Im}\left[\sum\mathcal{E}_n(z)\exp(i\psi_n)/2\gamma\right]\ . \tag{A11}$$

---

*Permanent address: IBS, LCCP, 41 avenue des Martyrs, 38027 Grenoble CEDEX 1, France.

[1] F. F. Chen, *Introduction to Plasma Physics* (Plenum, New York, 1974).

[2] D. Iracane and J.-L. Ferrer, Phys. Rev. Lett. **66**, 33 (1991).

[3] I. Kimel and L. R. Elias, Phys. Rev. A **35**, 3818 (1987).

[4] R. L. Tokar *et al.*, Nucl. Instrum. Methods Phys. Res. Sect. A **296**, 115 (1990).

[5] R. W. Warren *et al.*, Nucl. Instrum. Methods Phys. Res. Sect. A **285**, 1 (1989).

[6] T. M. Antonsen and B. Levush, Nucl. Instrum. Methods Phys. Res. A **272**, 472 (1988).

[7] D. Iracane and L. Bernis, Phys. Rev. A **42**, 6831 (1990).

[8] W. B. Colson, in *Free-Electron Generators of Coherent Radiation,* edited by C. A. Brau, SPIE Proc. Vol. 453 (SPIE, Bellingham, WA, 1984), p. 290.

[9] W. B. Colson, Phys. Rev. A **24**, 639 (1981).

[10] N. M. Kroll, P. L. Morton, and M. N. Rosenbluth, IEEE J. Quantum Electron. **QE-17**, 1436 (1981).

[11] E. T. Scharleman, A. M. Sessler, and J. S. Wurtele, Phys. Rev. Lett. **54**, 1925 (1985).

[12] S. Joly *et al.*, Nucl. Instrum. Methods Phys. Res. Sect. A **331**, 199 (1993).

[13] J. C. Goldstein, in *Free-Electron Generators of Coherent Radiation* (Ref. [8]), p. 2.

[14] D. C. Quimby, in *Free-Electron Lasers,* edited by B. E. Newman, SPIE Proc. Vol. 738 (SPIE, Bellingham, WA, 1987), p. 103, and references therein.

[15] W. B. Colson and S. K. Ride, Phys. Lett. **76A**, 379 (1980).

[16] W. B. Colson and R. A. Freedman, Opt. Commun. **46**, 37 (1983).

[17] G. Dattoli and A. Renieri, Nuovo Cimento B **61**, 153

(1981).
[18] H. Flocard, S. E. Koonin, and M. S. Weiss, Phys. Rev. C **17**, 1682 (1978); S. Koonin *et al.*, *ibid.* **15**, 1359 (1977).
[19] J. M. J. Madey, Nuovo Cimento B **50**, 64 (1979).
[20] G. Ramian, Nucl. Instrum. Methods Phys. Res. Sect. A **318**, 225 (1992).
[21] R. W. Warren, J. C. Goldstein, and B. E. Newman, Nucl. Instrum. Methods Phys. Res. Sect. A **250**, 19 (1986).
[22] J. C. Goldstein, B. E. Newman, and R. W. Warren, Nucl. Instrum. Methods Phys. Res. A **272**, 150 (1988).
[23] R. W. Warren and J. C. Goldstein, Nucl. Instrum. Methods Phys. Res. Sect. A **272**, 155 (1988).
[24] B. Hafizi, A. Ting, P. Sprangle, and C. M. Tang, Phys. Rev. A **38**, 197 (1988).
[25] J. L. Ferrer and D. Iracane, Nucl. Instrum. Methods Phys. Res. Sect. A **318**, 564 (1992).
[26] N. M. Kroll and M. N. Rosenbluth, in *Physics of Quantum Electronics,* edited by S. F. Jacobs *et al.* (Addison-Wesley, Reading, MA, 1980), Vol. 7, p. 147.
[27] D. W. Feldman *et al.*, Nucl. Instrum. Methods Phys. Res. Sect. A **285**, 11 (1989).
[28] A. Lichtenberg and M. Lieberman, *Regular and Stochastic Motion* (Springer-Verlag, Berlin, 1983).
[29] H. Risken, *The Fokker-Planck Equation* (Springer-Verlag, Berlin, 1984).
[30] R. Dautray and J. L. Lions, *Analyse Mathématique et Calcul Numérique pour les Sciences et les Techniques* (Masson, Paris, 1985).